EPJ manuscript No.
(will be inserted by the editor)

Meson Spectroscopy and Search for Spin-Exotic States at COMPASS*

Quirin Weitzel for the COMPASS Collaboration

Technische Universität München, Physik-Department E18, 85748 Garching, Germany
e-mail: qweitzel@e18.physik.tu-muenchen.de

Abstract. This paper presents the results of a partial wave analysis of about 420 000 diffractive dissociation events with four-momentum transfer $t' \in [0.1, 1]$ GeV$^2/c^2$. The data were recorded at COMPASS during a short pilot run in 2004, using a 190 GeV/c negative pion beam on lead targets. Reactions of the type $\pi^- N \to \pi^-\pi^-\pi^+ N'$ have been investigated and resonances up to 2.5 GeV/c^2 have been searched for. In addition to well-known mesons, also a state with spin-exotic quantum numbers $J^{PC} = 1^{-+}$ is observed.

1 Introduction

In the constituent quark model, mesons are characterized as bound states of a quark q and an antiquark $\bar{q}$. They are postulated to be color singlets and their total angular momentum J, parity P and charge conjugation C are given by

$$J = |L - S| \ldots |L + S| \quad , \quad P = (-1)^{L+1} \quad \text{and} \quad C = (-1)^{L+S} \quad . \tag{1}$$

Here L denotes the relative orbital angular momentum of the quark and antiquark, while S is their total intrinsic spin ($S = 0, 1$). In addition to J^{PC}, the isospin I and the G-parity are introduced, which are also conserved quantum numbers in strong interactions.

Quantum Chromo Dynamics (QCD) describes the interaction between colored quarks by the exchange of gluons g. Gluons carry color themselves which gives rise to a variety of new phenomena predicted by QCD. In particular, color-singlet mesons can be composed not only of $q\bar{q}$ pairs, but can contain other color-neutral configurations. In this context $qq\bar{q}\bar{q}$ tetraquarks, $q\bar{q}g$ hybrids and gg glueballs are mostly discussed [1]. They are, however, extremely difficult to find experimentally due to mixing with ordinary $q\bar{q}$ states. One prime goal of meson spectroscopy is therefore to search for so-called *spin-exotic* mesons which have quantum numbers forbidden in the quark model, thus violating the equations (1): e. g. $J^{PC} = 0^{--}, 0^{+-}, 1^{-+}$. The experimental observation of such states would provide a clear evidence of physics beyond the simple quark model and a fundamental confirmation of QCD.

The lowest-lying hybrid is expected to have quantum numbers $J^{PC} = 1^{-+}$. Lattice-QCD simulations [2] and flux-tube model calculations [3] predict a mass between 1.7 and 2.2 GeV/c^2, and a preferred decay into $b_1\pi$ and $f_1\pi$. On the experimental side two candidates for a 1^{-+} hybrid exist, $\pi_1(1400)$ and $\pi_1(1600)$, which are both still heavily disputed in the community. $\pi_1(1400)$ was mostly seen in $\eta\pi$ decays, e. g. by E852 [4], VES [5] and Crystal Barrel [6]. $\pi_1(1600)$ was observed by E852 and VES in $\rho\pi$ [7,8], $\eta'\pi$ [5,9], $f_1\pi$ [10,11] and $\omega\pi\pi$ [11,12]. Especially the $\rho\pi$ results from $\pi^-\pi^-\pi^+$ final-state events are controversially discussed [13,14], which calls for high-statistics experiments like COMPASS to shed new light on the situation.

* This work is supported by the German Bundesministerium für Bildung und Forschung (06MT244), the DFG cluster of excellence *Origin and Structure of the Universe* (EXC153), the Maier-Leibnitz-Labor der LMU und TU München, and CERN-RFBR grant 08-02-91009.

2 Diffractive Dissociation

One possible production mechanism for mesons is the diffractive dissociation of high-energetic projectiles on a fixed target. The corresponding reaction can be written down as

$$a + b \to c + d \qquad \text{with} \qquad c \to 1 + 2 + \cdots + n \quad , \tag{2}$$

where a is the incoming beam particle, b the target, c the produced meson system decaying into n particles and d the recoil particle. This is also illustrated in figure 1 (left). The reaction is a strong interaction and proceeds through a t-channel Reggeon exchange (mostly Pomeron, see e. g. [15]). It can be described by two kinematical variables, the squared center-of-mass energy $s = (p_a + p_b)^2$ and the square of the four-momentum transfer $t = (p_a - p_c)^2$. Usually $t' = |t| - |t|_{min}$ is introduced, where the minimum value of $|t|$ allowed for a given mass m_c is given in the center-of-mass frame by

$$|t|_{min} = 2(E_a E_c - |\mathbf{p}_a||\mathbf{p}_c|) - m_a^2 - m_c^2 \qquad \text{and} \qquad t' = 2|\mathbf{p}_a||\mathbf{p}_b|(1 - \cos\theta_0) \geq 0 \quad . \tag{3}$$

Here θ_0 denotes the scattering angle in the center-of-mass frame. On the right of figure 1 the special case of pion dissociation on a lead target is depicted, where the produced systems X (of mass m_c) decay into $\pi^-\pi^-\pi^+$ final states.

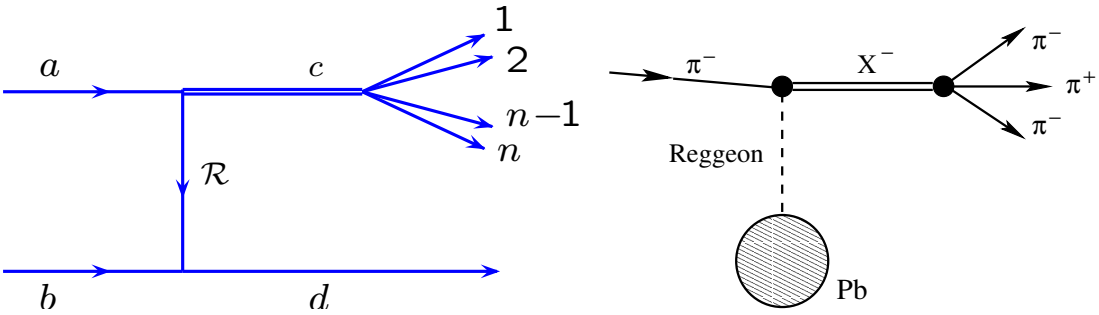

Fig. 1. Illustration of meson production from diffractive dissociation processes.

3 The COMPASS Experiment

COMPASS (COmmon Muon and Proton Apparatus for Structure and Spectroscopy) [16] is a fixed-target experiment at the CERN SPS, which investigates the structure and the spectrum of hadrons. In a first phase between 2002 and 2007, the spin structure of nucleons was measured by deep-inelastic scattering of 160 GeV/c muons off a polarized LiD or NH_3 target [17]. The second phase started in 2008 and is mostly dedicated to light-meson spectroscopy. Hadron beams of up to 280 GeV/c and a 40 cm long liquid-hydrogen target or thin (∼mm) disks of solid target material are used for this physics program. Outgoing particles are detected by a two-stage spectrometer, which covers a large range of scattering angles and particle momenta. Both stages are equipped with a dipole magnet and several types of tracking detectors. Particle identification is performed using a Ring Imaging Cherenkov (RICH) counter as well as hadronic and electromagnetic calorimetry [18].

3.1 The 2004 Pilot Hadron Run

In order to study the capability of COMPASS to measure diffractively produced mesons, a short pilot run took place in 2004. A 190 GeV/c π^- beam was used and, since in parallel Primakoff

reactions were studied, mostly lead targets were employed. The beam spot at the COMPASS target had a typically spread of about $3 \times 3\,\mathrm{mm}^2$ and the beam intensity was of the order of a few 10^6 particles/s. The targets were simple disks with a thickness of 1-2 mm. A dedicated trigger was set up to trigger on interactions with at least two outgoing charged particles. In addition, an online data-filtering process enhanced the fraction of diffractive events by requiring a certain hit multiplicity in the tracking stations right after the target. During the 2004 pilot run, no recoil particle detector around the target was yet available. The RICH counter was on purpose not active and the rather heavy chamber gas replaced by nitrogen to save material and avoid secondary interactions and photon conversions.

4 Data Sample and Acceptance

The results presented in this paper are based on about two days of data taking with the 2004 COMPASS pilot-run setup (cf. section 3.1). Primary vertices with one incoming negative and three outgoing $(-,-,+)$ particles are required in the offline analysis [19]. An exclusivity cut ensures that, taking into account also the momentum transfer t' according to equation (3), the total energy of the three outgoing pions sums up to the beam energy. More precisely, the beam energy E_a (see figure 1) has been calculated from the total energy E_c of the 3π system and the scattering angle θ_0, assuming that the target particle remained intact during the scattering process. The cut has been applied as $|E_a - 189| < 4\,\mathrm{GeV}$. More than 4 000 000 exclusive events have been obtained, covering values of t' between 0 and a few GeV^2/c^2.

For the following partial wave analysis (PWA) a t' range of $0.1 < t' < 1.0\,\mathrm{GeV}^2/c^2$ has been chosen, since there the discussed $\pi_1(1600)$ signals were observed in the past [13]. At such high values of t' scattering on the nucleons inside the lead nuclei dominates. The final event sample comprises about 420 000 events. Figure 2 (left) presents the invariant 3π mass spectrum, which exhibits the dominantly produced mesons $a_1(1260)$, $a_2(1320)$ and $\pi_2(1670)$. On the right of the same figure the (non-squared) Dalitz plot for the $\pi_2(1670)$ mass region is shown, visualizing the $\rho\pi$ (31% branching ratio) and the $f_2\pi$ (56%) decay modes.

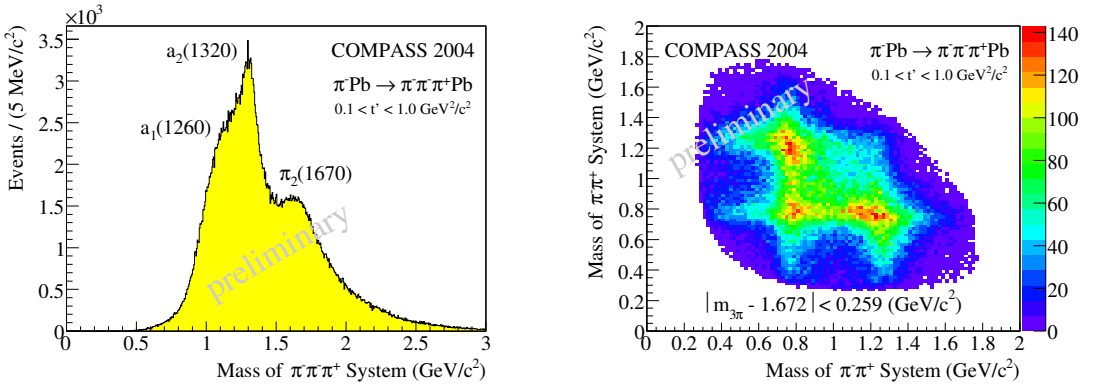

Fig. 2. Invariant mass of $\pi^-\pi^-\pi^+$ final states for $0.1 < t' < 1.0\,\mathrm{GeV}^2/c^2$ (left) and Dalitz plot for $\pi_2(1670)$, selected by a $\pm 1\Gamma$ cut around its nominal mass (right).

In order to be able to apply acceptance corrections for the PWA, the COMPASS 2004 hadron-run setup was simulated. Phase space distributed 3π Monte-Carlo events were generated with input from the real data and processed through the whole reconstruction and selection chain. On an event-by-event basis the acceptance has been worked out and provided to the PWA program (see section 5). For illustration, the COMPASS acceptance is shown in figure 3 as a function of the 3π mass (left) and of the polar angle of $\pi^+\pi^-$ pairs (their total momentum) in the Gottfried-Jackson frame (GJF). The GJF is defined as the 3π rest system, with the z axis along the beam particle direction and the y axis perpendicular to the production plane.

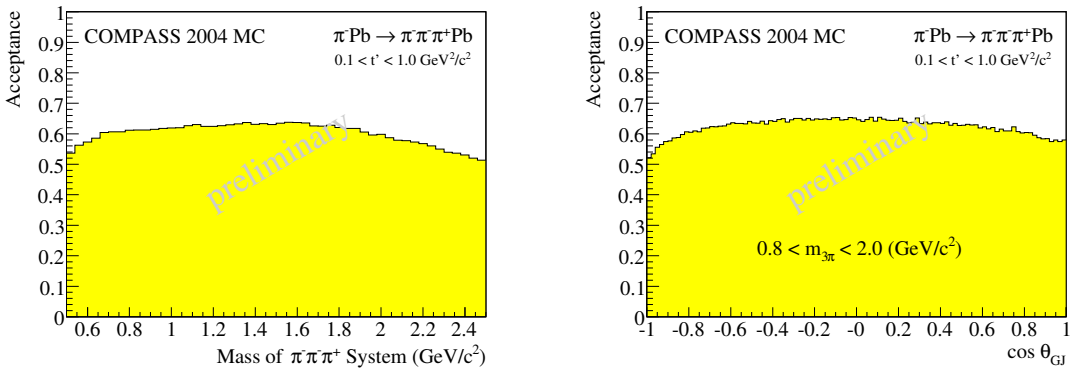

Fig. 3. Acceptance for diffractive events as a function of 3π mass (left) and $\cos\theta_{GJ}$ (right, see text).

5 Partial Wave Analysis

Based on the data set introduced in section 4, a partial wave analysis (PWA) has been performed using a program which was developed at Illinois [20] and later on modified at Protvino and Munich. The underlying formalism is built on two basic assumptions, namely the *isobar model* and the factorization of the total cross-section into a resonance and a recoil vertex. This is illustrated in figure 4: The diffractively produced resonance X with quantum numbers J^{PC} decays in a two-step process into three charged pions, without any further final-state interactions (within the pions or with the target). The decay proceeds through an intermediate di-pion resonance $R_{\pi\pi}$, called *isobar*, which decays strongly into a $\pi^+\pi^-$ pair. The isobar has spin S and relative orbital angular momentum L (with respect to the bachelor π^-), where L and S are coupled to J in the usual way. Also the spin projection of X is specified, by $M \geq 0$ and the reflectivity $\epsilon = \pm 1$ [21]. It should be noticed that $\epsilon = +1$ corresponds to natural parity exchange, like for e. g. Pomeron-mediated reactions. A *partial wave* is defined in the following by specifying the full set of quantum numbers $J^{PC}M^{\epsilon}[isobar\ \pi]L$. I and G (cf. section 1) are not explicitly denoted, since they have to be conserved at the resonance vertex and are therefore fixed by the incoming pion to $I^G = 1^-$. The goal of the PWA is to find and disentangle all resonances present in the data, and to determine their properties. For practical reasons this task is split into two steps, the *mass-independent PWA* and the *mass-dependent fit* [19].

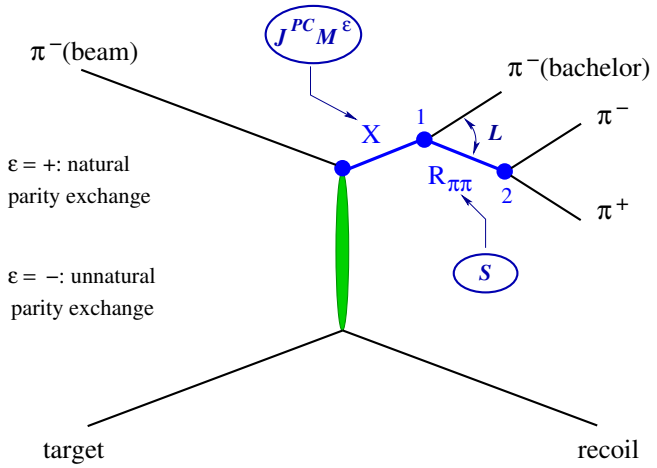

Fig. 4. Overview of quantum numbers describing a partial wave within the isobar model (see text).

5.1 Mass-Independent PWA

In this step, a fit of the data distributions in 3π phase space τ is performed in $40\,\mathrm{MeV}/c^2$ bins of the 3π mass $m = m_c$. No mass-dependent parameterizations are yet introduced for the produced resonances X (see figure 4), and the cross-section is written as

$$\sigma_{indep}(\tau, m) = \sum_{\epsilon=\pm1} \sum_{r=1}^{N_r} \left| \sum_i T_{ir}^{\epsilon} \psi_i^{\epsilon}(\tau, m) \Big/ \sqrt{\int |\psi_i^{\epsilon}(\tau', m)|^2 \mathrm{d}\tau'} \right|^2 \quad . \tag{4}$$

Here ψ_i^{ϵ} denotes the decay amplitude of a particular partial wave i. The fitting parameters T_{ir}^{ϵ} are called *production amplitudes*, since they contain the information about the strength of the waves and their interferences. Because of parity conservation, amplitudes with different ϵ are not allowed to interfere (in case of an unpolarized target). A further incoherence built-in to equation (4) is due to the *rank* N_r [21]: Assuming that in the analyzed t' range both the target and the recoil are nucleons, helicity-flip and non-flip amplitudes are foreseen for the baryon vertex ($N_r = 2$). The t' dependence of the cross-section is taken into account by multiplying different functions of t', which are obtained from the data, to the decay amplitudes ψ_i^{ϵ}.

A total of 42 partial waves is used in the mass-independent PWA (see table 1), including five different isobars: $(\pi\pi)_s$ (broad $\sigma(600)$ and $f_0(1370)$, see [13]), $\rho(770)$, $f_0(980)$, $f_2(1270)$ and $\rho_3(1690)$. Mostly $\epsilon = +1$ amplitudes are needed to describe the data. A background wave, which is flat in the relevant GJF angles, is added incoherently. It receives less than 10% of the total intensity. The complex numbers T_{ir}^{ϵ} are obtained using an extended maximum-likelihood method, respecting the experimental acceptance (cf. section 4). In section 5.3 the mass-independent fit results are presented as black data points with statistical error bars. In fact 30 independent fit attempts with random start parameters have been performed for each mass bin, from which the best one in terms of $\ln \mathcal{L}$ is chosen. If two or more solutions are obtained within one unit of $\ln \mathcal{L}$, the statistical error for that mass bin is increased as indicated by a thick green bar.

$J^{PC}M^{\epsilon}$	L	Isobar π	Cut (GeV/c^2)
$0^{-+}0^{+}$	S	$f_0\pi$	1.40
$0^{-+}0^{+}$	S	$(\pi\pi)_s\pi$	-
$0^{-+}0^{+}$	P	$\rho\pi$	-
$1^{-+}1^{+}$	P	$\rho\pi$	-
$1^{++}0^{+}$	S	$\rho\pi$	-
$1^{++}0^{+}$	P	$f_2\pi$	1.20
$1^{++}0^{+}$	P	$(\pi\pi)_s\pi$	0.84
$1^{++}0^{+}$	D	$\rho\pi$	1.30
$1^{++}1^{+}$	S	$\rho\pi$	-
$1^{++}1^{+}$	P	$f_2\pi$	1.40
$1^{++}1^{+}$	P	$(\pi\pi)_s\pi$	1.40
$1^{++}1^{+}$	D	$\rho\pi$	1.40
$2^{-+}0^{+}$	S	$f_2\pi$	1.20
$2^{-+}0^{+}$	P	$\rho\pi$	0.80
$2^{-+}0^{+}$	D	$f_2\pi$	1.50
$2^{-+}0^{+}$	D	$(\pi\pi)_s\pi$	0.80
$2^{-+}0^{+}$	F	$\rho\pi$	1.20
$2^{-+}1^{+}$	S	$f_2\pi$	1.20
$2^{-+}1^{+}$	P	$\rho\pi$	0.80
$2^{-+}1^{+}$	D	$f_2\pi$	1.50
$2^{-+}1^{+}$	D	$(\pi\pi)_s\pi$	1.20
$2^{-+}1^{+}$	F	$\rho\pi$	1.20
$2^{++}1^{+}$	P	$f_2\pi$	1.50
$2^{++}1^{+}$	D	$\rho\pi$	-
$3^{++}0^{+}$	S	$\rho_3\pi$	1.50
$3^{++}0^{+}$	P	$f_2\pi$	1.20
$3^{++}0^{+}$	D	$\rho\pi$	1.50
$3^{++}1^{+}$	S	$\rho_3\pi$	1.50
$3^{++}1^{+}$	P	$f_2\pi$	1.20
$3^{++}1^{+}$	D	$\rho\pi$	1.50
$4^{-+}0^{+}$	F	$\rho\pi$	1.20
$4^{-+}1^{+}$	F	$\rho\pi$	1.20
$4^{++}1^{+}$	F	$f_2\pi$	1.60
$4^{++}1^{+}$	G	$\rho\pi$	1.64
$1^{-+}0^{-}$	P	$\rho\pi$	-
$1^{-+}1^{-}$	P	$\rho\pi$	-
$1^{++}1^{-}$	S	$\rho\pi$	-
$2^{-+}1^{-}$	S	$f_2\pi$	1.20
$2^{++}0^{-}$	P	$f_2\pi$	1.30
$2^{++}0^{-}$	D	$\rho\pi$	-
$2^{++}1^{-}$	P	$f_2\pi$	1.30
FLAT			

Table 1. Overview of the 42 partial waves used for the mass-independent PWA fit (see text); the listed cuts are lower boundaries for the 3π mass from which on a particular wave is used.

5.2 Mass-Dependent Fit

In the second analysis step, the results from the mass-independent PWA are fitted by means of a mass-dependent model. Relativistic Breit-Wigner (BW) and eventually background functions are introduced, which describe the mass-dependence of the partial waves and of their interferences with each other [19]. A χ^2-fit is employed for this task. For the presented analysis, seven waves out of the initial 42 waves have been selected, including the most significant ones and those containing well-expressed resonances: $0^{-+}0^{+}[f_0(980)\pi]S$, $1^{-+}1^{+}[\rho\pi]P$ (spin-exotic), $1^{++}0^{+}[\rho\pi]S$, $2^{-+}0^{+}[f_2\pi]S$, $2^{-+}0^{+}[f_2\pi]D$, $2^{++}1^{+}[\rho\pi]D$ and $4^{++}1^{+}[\rho\pi]G$. From the χ^2-fit, which is shown in section 5.3 as red curve overlayed to the mass-independent PWA results, resonance masses and widths have been obtained. The $2^{-+}0^{+}[f_2\pi]D$ wave has optionally also been taken out from the analysis, since its nature is still unclear. The results, however, do not depend on the presence of this wave in the mass-dependent fit.

5.3 Results

Figure 5 presents for several partial wave intensities both the results from the mass-independent PWA and from the mass-dependent fit. From top to bottom and left to right the $1^{++}0^{+}[\rho\pi]S$, $2^{-+}0^{+}[f_2\pi]S$, $2^{++}1^{+}[\rho\pi]D$, $4^{++}1^{+}[\rho\pi]G$, $0^{-+}0^{+}[f_0(980)\pi]S$ and $1^{-+}1^{+}[\rho\pi]P$ intensities are shown. The first three correspond to the well-known $a_1(1260)$, $\pi_2(1670)$ and $a_2(1320)$ mesons. The forth and the fifth wave have low statistics, but still the $a_4(2040)$ and the $\pi(1800)$ are clearly seen. With a similar significance, a broad bump around $1.6\,\mathrm{GeV}/c^2$ is observed in the spin-exotic $1^{-+}1^{+}[\rho\pi]P$ wave (bottom, right). This signal is interpreted as the disputed hybrid candidate $\pi_1(1600)$ [7,13]. The phase of the interference term between the $1^{-+}1^{+}[\rho\pi]P$ wave and the $1^{++}0^{+}[\rho\pi]S$ and the $2^{-+}0^{+}[f_2\pi]S$ wave is presented on the left and right of figure 6, respectively. In particular the former exhibits a clean phase motion around $1.6\,\mathrm{GeV}/c^2$, which demonstrates the resonance nature of the 1^{-+} signal. The absence of a phase motion in the second case is attributed to the fact that two resonances with similar mass and width, $\pi_2(1670)$ and $\pi_1(1600)$, dominate in the respective partial waves.

In addition to a Breit-Wigner (BW) resonance (blue line in figure 5 bottom, right), a non-resonant background (purple line) has been introduced in the mass-dependent fit to describe the low-mass shoulder in the $1^{-+}1^{+}[\rho\pi]P$ wave. On the level of available statistics it was not possible to identify the nature of these events. One possible explanation would be a Deck-like effect [22], which is known to be important for e. g. the $a_1(1260)$ decaying also into $\rho\pi$. For the systematic error estimate it was also tried to include a second resonance, possibly corresponding to $\pi_1(1400)$, in the mass-dependent fit. However, only with fixed parameters for this second BW the fit became stable. A third possibility would be leakage from one of the dominant waves to the 1^{-+} wave. A dedicated study was therefore carried out based on Monte-Carlo events. The parameters of the 16 most dominant partial waves, obtained from a mass-dependent fit, were used to generate the events, excluding the 1^{-+}. They were passed through a full simulation of the COMPASS setup, reconstructed and analyzed by the same PWA technique and model as used for the real data. The total leakage to the spin-exotic wave was found to be less than 5%, which is negligible.

Table 2 summarizes the obtained parameters for all presented resonances. Both masses and widths are stated together with the respective statistical and systematic errors. The latter have been obtained from a series of studies [19], during which for example the wave set and the mass-thresholds in the mass-independent PWA were varied. Also different isobar parameterizations were tried and selection cuts were modified. Concerning the mass-dependent fit, the model was changed in many regards. Mentionable are the very asymmetric errors on the width of $a_2(1320)$, on the mass of $a_4(2040)$ and on the mass of $\pi_1(1600)$. In the first case the effect of the experimental mass resolution was estimated, while in the second case the influence of the BW type was tested (constant width vs. dynamic width). The systematic error on the $\pi_1(1600)$ mass takes into account the possibility of having also an interfering $\pi_1(1400)$ in the 1^{-+} wave (see also above).

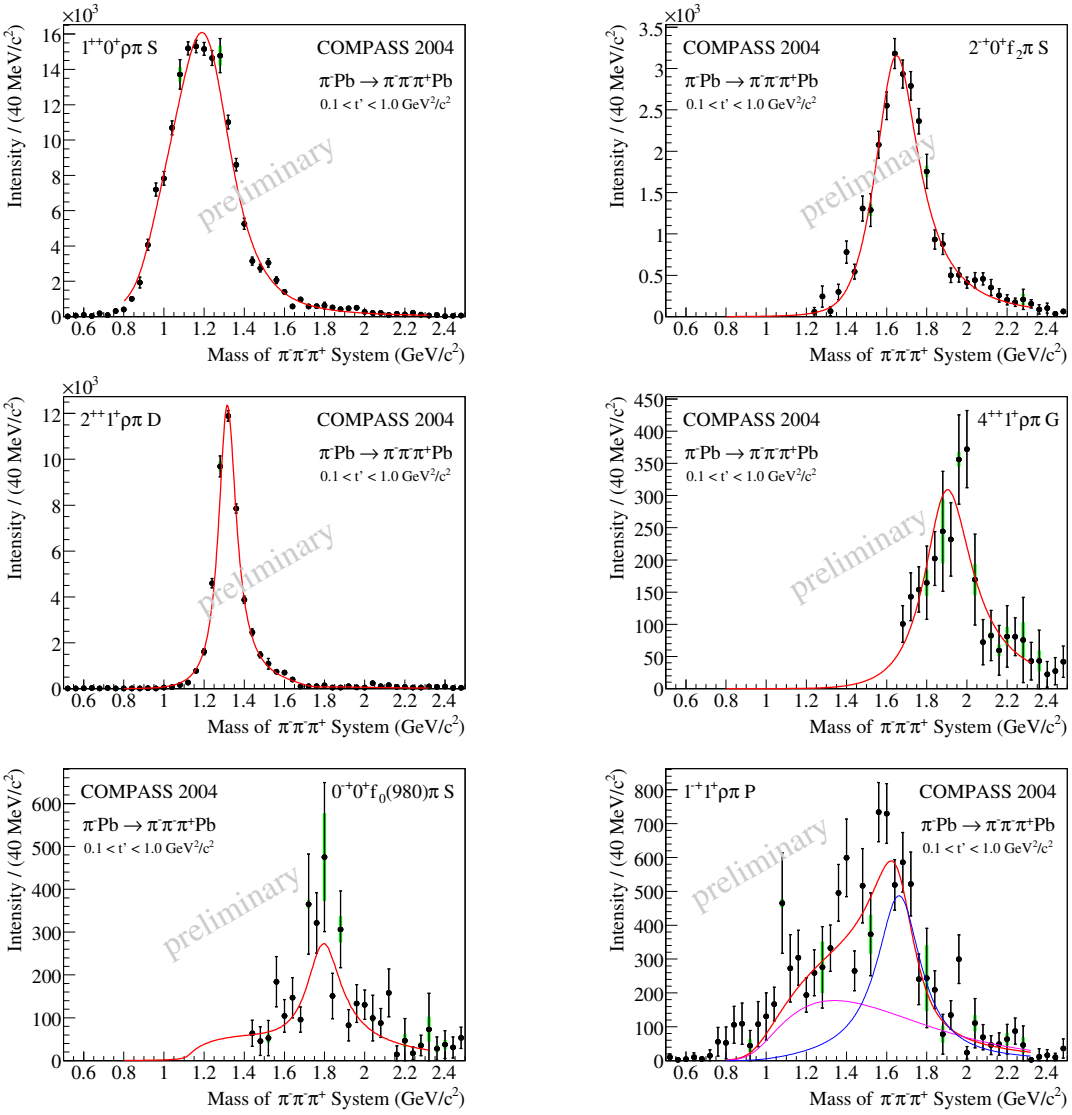

Fig. 5. Partial wave intensities (black points) and result of mass-dependent fit (red curve).

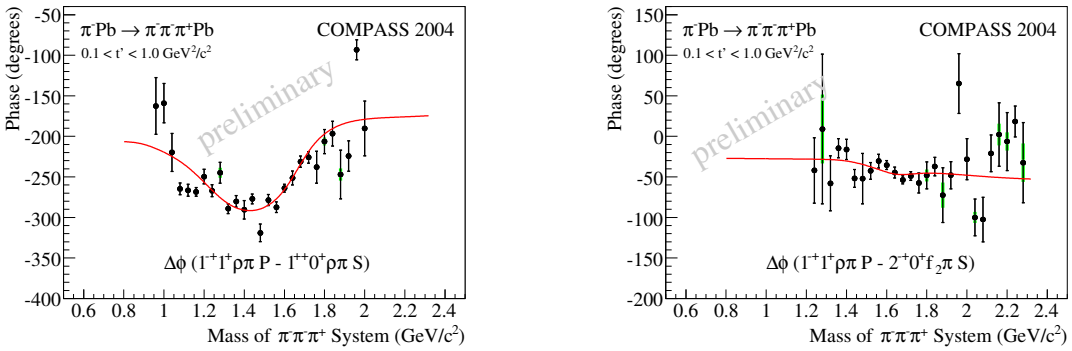

Fig. 6. Phase of the $1^{-+}1^{+}[\rho\pi]P$ wave w. r. t. the $1^{++}0^{+}[\rho\pi]S$ and the $2^{-+}0^{+}[f_2\pi]S$ wave.

State	Mass ± stat. +− syst. (GeV/c^2)	Width ± stat. +− syst. (GeV/c^2)
$a_1(1260)$	1.256 ± 0.006 + 0.007 - 0.017	0.366 ± 0.009 + 0.028 - 0.025
$a_2(1320)$	1.321 ± 0.001 + 0.000 - 0.007	0.110 ± 0.002 + 0.002 - 0.015
$\pi_1(1600)$	1.660 ± 0.010 + 0.000 - 0.064	0.269 ± 0.021 + 0.042 - 0.064
$\pi_2(1670)$	1.659 ± 0.003 + 0.024 - 0.008	0.271 ± 0.009 + 0.022 - 0.024
$\pi(1800)$	1.785 ± 0.009 + 0.012 - 0.006	0.208 ± 0.022 + 0.021 - 0.037
$a_4(2040)$	1.884 ± 0.013 + 0.050 - 0.002	0.295 ± 0.024 + 0.046 - 0.019

Table 2. Resonance masses and widths with statistical and systematic errors; preliminary.

6 Summary and Outlook

Diffractive dissociation reactions at COMPASS provide clean access to meson resonances in the light-quark sector. One of the prime goals of the spectroscopy program is to search for states with gluonic degrees of freedom, in particular to shed light on the disputed hybrid candidates $\pi_1(1400)$ and $\pi_1(1600)$. During a short pilot run in 2004 several million exclusive $\pi^-\pi^-\pi^+$ events were recorded using a 190 GeV/c π^- beam and lead targets. A partial wave analysis of a subset of this data, with momentum transfers $t' \in [0.1, 1.0]\,\mathrm{GeV}^2/c^2$, has been performed. Several established mesons with masses below $2\,\mathrm{GeV}/c^2$ are confirmed and, in addition, a resonance with spin-exotic quantum numbers $J^{PC} = 1^{-+}$ is observed. A mass-dependent fit yields a mass and width of $1.660^{+0.010}_{-0.074}$ and $0.269^{+0.063}_{-0.085}\,\mathrm{GeV}/c^2$ (statistical and systematic errors added linearly), respectively, which is consistent with the reported $\pi_1(1600)$.

In 2008 a full beam time dedicated to meson spectroscopy took place, from which an increase in statistics of two orders of magnitude can be expected for $\pi^-\pi^-\pi^+$ events. A liquid-hydrogen target was employed, and a recoil particle detector was installed to enhance the fraction of diffractive events. With this data the hybrid search can be extended to the mass range above $2\,\mathrm{GeV}/c^2$, which is still covered by the excellent acceptance of COMPASS. In addition, data were also taken to study meson production from K^- dissociation and from central production reactions.

References

1. E. Klempt and A. Zaitsev, Phys. Rept. **454**, (2007) 1.
2. C. McNeile and C. Michael, Phys. Rev. **D73**, (2006) 074506.
3. F. E. Close and P. R. Page, Nucl. Phys. **B443**, (1995) 233.
4. D. R. Thompson et al., Phys. Rev. Lett. **79**, (1997) 1630.
5. G. M. Beladidze et al., Phys. Lett. **B313**, (1993) 276.
6. A. Abele et al., Phys. Lett. **B423**, (1998) 175.
7. G. S. Adams et al., Phys. Rev. Lett. **81**, (1998) 5760.
8. Y. Khokhlov, Nucl. Phys. **A663**, (2000) 596.
9. E. I. Ivanov et al., Phys. Rev. Lett **86**, (2001) 3977.
10. J. Kuhn et al., Phys. Lett. **B595**, (2004) 109.
11. D. V. Amelin et al., Phys. Atom. Nucl. **68**, (2005) 359.
12. M. Lu et al., Phys. Rev. Lett. **94**, (2005) 032002.
13. S. U. Chung et al., Phys. Rev. **D65**, (2002) 072001.
14. A. R. Dzierba et al., Phys. Rev. **D73**, (2006) 072001.
15. U. Amaldi, M. Jacob and G. Matthiae, Ann. Rev. Nucl. Part. Sci. **26**, (1976) 385.
16. P. Abbon et al., Nucl. Instrum. Meth. **A577**, (2007) 455.
17. Y. Kiselev et al., *in these proceedings*, (2008).
18. F. Nerling for the COMPASS Collaboration, *in these proceedings*, (2008).
19. Q. Weitzel, PhD Thesis, TU München, Physik-Department E18, (2008).
20. J. D. Hansen et al., Nucl. Phys. **B81**, (1974) 403.
21. S. U. Chung and T. L. Trueman, Phys. Rev. **D11**, (1975) 633.
22. R. T. Deck, Phys. Rev. Lett. **13**, (1964) 169.